Published in final edited form as:
Proc Soc Photo Opt Instrum Eng. 2014 March 21; 9034: 90340Y–. doi:10.1117/12.2036497.

Improved Statistical Power with a Sparse Shape Model in Detecting an Aging Effect in the Hippocampus and Amygdala

Moo K. Chung[1,*], **Seung-Goo Kim**[2], **Stacey M. Schaefer**[1], **Carien M. van Reekum**[3], **Lara Peschke-Schmitz**[1], **Matthew J. Sutterer**[4], and **Richard J. Davidson**[1]

[1]University of Wisconsin-Madison, USA

[2]Max Planck Institute, Germany

[3]University of Reading, UK

[4]University of Iowa, USA

Abstract

The sparse regression framework has been widely used in medical image processing and analysis. However, it has been rarely used in anatomical studies. We present a sparse shape modeling framework using the Laplace-Beltrami (LB) eigenfunctions of the underlying shape and show its improvement of statistical power. Traditionally, the LB-eigenfunctions are used as a basis for intrinsically representing surface shapes as a form of Fourier descriptors. To reduce high frequency noise, only the first few terms are used in the expansion and higher frequency terms are simply thrown away. However, some lower frequency terms may not necessarily contribute significantly in reconstructing the surfaces. Motivated by this idea, we present a LB-based method to filter out only the significant eigenfunctions by imposing a sparse penalty. For dense anatomical data such as deformation fields on a surface mesh, the sparse regression behaves like a smoothing process, which will reduce the error of incorrectly detecting false negatives. Hence the statistical power improves. The sparse shape model is then applied in investigating the influence of age on amygdala and hippocampus shapes in the normal population. The advantage of the LB sparse framework is demonstrated by showing the increased statistical power.

1. INTRODUCTION

There have been many basis function based shape representations such as Fourier descriptors,[20] spherical harmonic representation,[4, 18, 21] wavelets,[2, 8, 9] wavelets[13, 25] and Laplace-Beltrami eigenfunction methods.[11, 14, 16, 17] These methods parameterize the coordinates of an object as a series expansion involving the basis functions. These basis representations do not selectively pick basis in reconstructing shapes. Usually the first few terms are used in the expansion and higher frequency terms are truncated. However, some lower frequency terms may not necessarily contribute significantly in reconstructing the shape while high frequency terms are actually important. Motivated by this simple idea, we

Send correspondence to: Moo K. Chung, 1500 Highland Ave. #281, Madison, WI. 53705, USA. mkchung@wisc.edu.

developed a new sparse shape modeling framework that selectively filters out basis functions.

In order to show the improved performance of the proposed shape representation, we introduce the statistical power analysis framework, where the minimum sample size requirement for discriminating between the groups is used as a criterion for the performance. Since the statistical power has to be computed along every point in the anatomical structure, it introduces a multiple comparisons problem.[6] Currently there is *no* anatomical study that shows how to perform the power analysis under multiple comparisons. We show the proposed sparse shape model can improve the power by 9.1%, which is considered as significant.

The proposed method is subsequently applied in characterizing aging in the hippocampus and amygdala. The main contributions of this paper are the introductions of (1) the new sparse shape model using the intrinsic Laplace-Beltrami eigenfunctions and (2) the new power analysis framework under multiple comparisons.

2. SPARSE SHAPE REPRESENTATION

Consider a real-valued functional measurement $Y(p)$ on a manifold $\mathcal{M} \subset \mathbb{R}^3$. Y can be vectors such as surface displacement or coordinates or scalars such as length of displacement. Then we assume the following additive model:

$$Y(p)=\theta(p)+\varepsilon(p), \quad (1)$$

where $\theta(p)$ is the unknown mean signal to be estimated and $\varepsilon(p)$ is a zero-mean Gaussian random field. For the Laplace-Beltrami (LB) operator Δ of $\mathcal{M}$, the natural intrinsic basis functions are obtained by solving

$$\Delta\psi_j=\lambda_j\psi_j, \quad (2)$$

where the eigenfunctions ψ_j corresponding to the eigenvalues λ_j form an orthonormal basis in $L^2(\mathcal{M})$, the space of square integrable functions on $\mathcal{M}$. We may order eigenvalues as $0 = \lambda_0 \le \lambda_1 \le \lambda_2 \cdots$ and corresponding eigenfunctions as $\psi_0, \psi_1, \psi_2, \cdots$. Since LB-operator on an arbitrary curved surface is unknown, the eigenfunctions are numerically estimated by discretizing the LB-operator using the Cotan discretization.[3,5,14] The first six LB-eigenfunctions are shown in Figure 1.

Using the eigenfunctions ψ_j, we can parametrically estimate the unknown mean signal $\theta(p)$ as the Fourier expansion:

$$\hat{\theta}(p)=\sum_{i=0}^{k}\beta_j\psi_j,$$

where β_j are the Fourier coefficients to be estimated. The Fourier coefficients can be obtained by the usual least squares estimation (LSE) by solving $\mathbf{Y} = \boldsymbol{\psi}\boldsymbol{\beta}$, where $\mathbf{Y} = (Y(p_1),$

$\cdots, Y(p_n))'$, $\boldsymbol{\beta} = (\beta_1, \cdots, \beta_k)'$ and $\boldsymbol{\psi} = (\psi_i(p_j))$ is an $n \times k$ matrix of eigenfunctions evaluated at mesh vertices. The Fourier coefficients $\boldsymbol{\beta}$ are then estimated as

$$\hat{\boldsymbol{\beta}} = (\boldsymbol{\psi}'\boldsymbol{\psi})^{-1}\boldsymbol{\psi}'\mathbf{Y}. \quad (3)$$

In most basis representation techniques using LB-eigenfunctions or spherical harmonics (SPHARM), only the first few terms are used in the expansion and higher frequency terms are simply thrown away to reduce the high frequency noise.[14,21] For example, between 12 and 15 degree SPHARM expansions have been used for hippocampus and caudate surfaces.[21] However, some lower frequency terms may not necessarily contribute significantly in reconstructing the surfaces. Motivated by this idea, we propose to sparsely filter out insignificant eigenfunctions by imposing the additional L_1-norm penalty to sparsely filter out insignificant low degree coefficients. Following,[7] L_1-estimation is given by

$$\hat{\boldsymbol{\beta}} = \min_{\boldsymbol{\beta}} ||\mathbf{Y} - \boldsymbol{\psi}\beta||_2^2 + \lambda||\boldsymbol{\beta}||_1, \quad (4)$$

where the parameter $\lambda > 0$ controls the amount of sparsity. Figure 2 shows an example of the shape representation where surface coordinates are sparsely filtered out.

3. STATISTICAL POWER UNDER MULTIPLE COMPARISONS

The effect of the sparse shape model is quantified using the power analysis. Power analysis is rarely done in anatomical studies and usually does not account for interdependency of voxels.[6,10] In this paper, we show how to perform the power analysis under spatial dependency of voxels, a multiple comparisons problem. We demonstrate that the proposed model can boost the statistical power.

The usual hypotheses for testing the significance of the signal in the model (1) under multiple comparisons are given by

$$H_0: \theta(p) = 0 \text{ for all } p \in \mathscr{M} \text{ vs. } H_1: \theta(p) > 0 \text{ for some } p \in \mathscr{M}.$$

Given a procedure for testing for the significance of θ, the type-I error (denoted as *agr;*) is the probability of rejecting H_0 when H_0 is true, i.e. *agr;* = P(reject H_0 | H_0 true). On the other hand, the type-II error (denoted as β) is the probability of not rejecting H_0 when H_0 is false, i.e. $\beta = P$(not reject H_0 | H_0 false). The *power* $\mathcal{P}$ of the procedure is defined as $1 - \beta$ and written as

$$\mathscr{P} = P(\text{reject } H_0 | H_1 \text{ true}).$$

The power is the probability of rejecting the null hypothesis that there is no signal when there is an actual signal. *When the test procedure has the power of 0.9, it implies that the method can correctly detect signal* 90% *of time when there is a real signal*. Statistical power is somewhat similar to classification accuracy in machine learning. The power is usually given in as a function of sample size. With an infinite number of samples, we can then achieve 100% power with any method. The statistical power is a good summary measure for numerically evaluating the performance of a method although it is rarely used in this fashion due to the difficulty of computing it under multiple comparisons.

3.1 Power under Multiple Comparisons

To compute the power over manifold $\mathcal{M}$, it is necessary to determine the type-I error first. Given a test random field $T(p)$, we reject H_0 if $T(p) > h$ for some thresholding h for all $p \in \mathcal{M}$. This is equivalent to the event $\sup_{p\in\mathcal{M}} T(p) > h$.[6] Hence, the type-I error over $\mathcal{M}$ is given by

$$\alpha = P\left(\sup_{p\in\mathcal{M}} T(p) > h\right).$$

The rejection region is taken as the subset of $\mathcal{M}$ (Figure 3):

$$\mathcal{M}_1 = \{x \in \mathcal{M} | T(x) > h\}.$$

Then the over all statistical power $\mathcal{P}$ is computed as

$$\mathcal{P} = P\left(\sup_{t\in\mathcal{M}} T(t) > h \middle| H_1\right). \quad (5)$$

4. EXPERIMENTAL RESULTS

As part of an ongoing study on midlife in the US (MIDUS II; http://midus.wisc.edu),[23] we have high-resolution T1-weighted inverse recovery fast gradient echo MRI, collected in 124 contiguous 1.2-mm axial slices (TE=1.8 ms; TR=8.9 ms; flip angle = 10°; FOV = 240 mm; 256 × 256 data acquisition matrix) of 69 middle-age and elderly adults ranging between 38 to 79 years (mean age = 58.0 ± 11.4 years). There are 23 men and 46 women in the study. Trained raters manually segmented the left and right amygdala and hippocampus separately. Brain tissues in the MRI scans were automatically segmented using Brain Extraction Tool (BET).[19] Then we performed a nonlinear image registration using the diffeomorphic shape and intensity averaging technique with the cross-correlation as the similarity metric through Advanced Normalization Tools (ANTS).[1] An initial template was constructed from a random subsample of 10 subjects. Using the deformation field obtained from warping the individual image to the template, we aligned the amygdala and hippocampus binary masks to the template space. The normalized masks were then averaged to produce the final study template. The isosurface of the template was extracted using the marching cube algorithm.[12] The displacement vector field is defined on each voxel, while the vertices of mesh are

located within a voxel. Thus we linearly interpolated the vector field on mesh vertices from the voxels.

4.1 Sparse Shape Analysis

The length of displacement vector field along the template surface was estimated using the sparse framework with $\lambda = 1$ and $k = 1000$ eigenfunctions. This is a sufficient number of basis functions to represent amygdala and hippocampus surfaces. Only 5% of the largest coefficients among 1000 estimated coefficients are used in the sparse representation, which has an effect of smoothing out noisy displacements. The age effect on the displacement length is regressed over the total brain volume and other variables:

$$\text{length} = \beta_1 + \beta_2 \cdot \text{brain} + \beta_3 \cdot \text{age} + \beta_4 \cdot \text{gender} + \varepsilon, \quad (6)$$

where ε is a zero mean Gaussian field. The age effect was determined by performing a T-test on the parameter β_3. The results are displayed in Figure 4. We found the regions of highly significant effects of age on the posterior part of the hippocampi (corrected p-value < 0.05). Particularly on the tail regions of the left and right hippocampi, we found highly localized age effects which are consistent with other shape modeling studies on the hippocampus.[15,24] We did not find any age effects on the amygdala surface.

4.2 Power Computation by Resampling

The direct power computation using the random field theory requires estimating the smoothness of signal, which is not trivial.[6] Instead we propose a resampling technique. First, we need to identify the threshold h corresponding to a specific *agr;*-level. For T-random field $T(x)$, the threshold h corresponding to the type-I error at 0.05 is given by

$$P\left(\sup_{x \in \mathcal{M}} T(x) > h\right) = 0.05,$$

where $\mathcal{M}$ is the surface of interest. For the power computation, it is needed to identify the rejection region $\mathcal{M}_1$ as well. The rejection region is taken as the subset of $\mathcal{M}$:

$$\mathcal{M}_1 = \{x \in \mathcal{M} | T(x) > h\}.$$

Then the over all statistical power $\mathcal{P}$ is computed as

$$\mathcal{P} = P\left(\sup_{x \in \mathcal{M}_1} T(x) > h\right),$$

where the supremum is restricted to the rejection region $\mathcal{M}_1$ (Figure 4). The thresholds h corresponding to *agr;* = 0.05 for the left and right hippocampi are 3.71 and 3.77. The resampling based power computation is performed as follows.

1. Set the counter $c = 0$.
2. Randomly pick n subjects out of total 69 subjects.
3. For n subjects, perform GLM (6) and obtain the t-statistic values in $\mathcal{M}_1$.
4. If any t-static value is larger than h, increase the counter $c \leftarrow c + 1$.
5. Repeat the above procedures $m = 5000$ times.

The frequency of rejection c/m approximates the power $\mathcal{P}$ as m becomes large for the given sample size n. 5000 resamples are sufficient to guarantee the robust estimation of the power. The resulting power is plotted as a function of sample size (Figure 5). In the right hippocampus, we have an increase of 0.091 in statistical power at the sample size 50. This implies that the proposed sparse model can increase the accuracy of detection by up to 9.1% in smaller sample studies.

5. CONCLUSION

We have presented a new sparse shape modeling framework using the Laplace-Beltrami eigenfunctions. The proposed framework is demonstrated to increase the statistical power by up to 9.1%. The significant structural changes found on hippocampi due to normal aging is consistent with the previous hippocampus shape analyses.[15,22]

Acknowledgments

This research was supported by the National Institute on Aging (PO1-AG020166) and the National Institute on Mental Health (R01 MH043454), the Waisman Intellectual and Developmental Disabilities Research Center (Waisman IDDRC), P30HD03352, and the Vilas Associate Award from the University of Wisconsin-Madison.

References

1. Avants BB, Epstein CL, Grossman M, Gee JC. Symmetric diffeomorphic image registration with cross-correlation: Evaluating automated labeling of elderly and neurodegenerative brain. Medical image analysis. 2008; 12:26–41. [PubMed: 17659998]
2. Bernal-Rusiel J, Atienza M, Cantero J. Detection of focal changes in human cortical thickness: spherical wavelets versus gaussian smoothing. NeuroImage. 2008; 41:1278–1292. [PubMed: 18474434]
3. Chung, MK. PhD Thesis. McGill University; 2001. Statistical Morphometry in Neuroanatomy.
4. Chung MK, Hartley R, Dalton KM, Davidson RJ. Encoding cortical surface by spherical harmonics. Satistica Sinica. 2008; 18:1269–1291.
5. Chung, MK.; Taylor, J. Diffusion smoothing on brain surface via finite element method. Proceedings of IEEE International Symposium on Biomedical Imaging (ISBI); 2004. p. 432-435.
6. Hayasaka S, Peiffer AM, Hugenschmidt CE, Laurienti PJ. Power and sample size calculation for neuroimaging studies by non-central random field theory. NeuroImage. 2007; 37:721–730. [PubMed: 17658273]
7. Kim SJ, Koh K, Lustig M, Boyd S, Gorinevsky D. An interior-point method for large-scale l1-regularized least squares. IEEE Journal of Selected Topics in Signal Processing. 2007; 1:606–617.
8. Kim WH, Pachauri D, Hatt C, Chung MK, Johnson S, Singh V. Wavelet based multi-scale shape features on arbitrary surfaces for cortical thickness discrimination. Advances in Neural Information Processing Systems (NIPS). 2012; 25:1250–1258.
9. Laga, H.; Takahashi, H.; Nakajima, M. Spherical wavelet descriptors for content-based 3D model retrieval. IEEE International Conference on Shape Modeling and Applications (SMI); 2006. p. 15-15.

10. Lerch JP, Evans AC. Cortical thickness analysis examined through power analysis and a population simulation. NeuroImage. 2005; 24:163–173. [PubMed: 15588607]
11. Lévy, B.; Inria-Alice, F. Laplace-beltrami eigenfunctions towards an algorithm that “understands” geometry. IEEE International Conference on Shape Modeling and Applications; 2006; 2006.
12. Lorensen, WE.; Cline, HE. Marching cubes: A high resolution 3D surface construction algorithm. Proceedings of the 14th annual conference on Computer graphics and interactive techniques; 1987. p. 163-169.
13. Nain D, Haker S, Bobick A, Tannenbaum A. Multiscale 3-D shape representation and segmentation using spherical wavelets. IEEE Transactions on Medical Imaging. 2007; 26:598–618. [PubMed: 17427745]
14. Qiu A, Bitouk D, Miller MI. Smooth functional and structural maps on the neocortex via orthonormal bases of the laplace-beltrami operator. IEEE Transactions on Medical Imaging. 2006; 25:1296–1396. [PubMed: 17024833]
15. Qiu A, Miller MI. Multi-structure network shape analysis via normal surface momentum maps. NeuroImage. 2008; 42:1430–1438. [PubMed: 18675553]
16. Reuter M, Biasotti S, Giorgi D, Patanè G, Spagnuolo M. Discrete laplace–beltrami operators for shape analysis and segmentation. Computers & Graphics. 2009; 33:381–390.
17. Seo, S.; Chung, MK.; Vorperian, HK. Heat kernel smothing using laplace-beltrami eigenfunctions. Medical Image Computing and Computer-Assisted Intervention – MICCAI 2010, volume 6363 of Lecture Notes in Computer Science; 2010. p. 505-512.
18. Shen, L.; Chung, MK. Large-scale modeling of parametric surfaces using spherical harmonics. Third International Symposium on 3D Data Processing, Visualization and Transmission (3DPVT); 2006.
19. Smith SM. Fast robust automated brain extraction. Human Brain Mapping. 2002; 17:143–155. [PubMed: 12391568]
20. Styner M, Oguz I, Smith R, Cascio C, Jomier M. Corpus callosum subdivision based on a probabilistic model of inter-hemispheric connectivity. Medical Image Computing and Computer Assisted Intervention (MICCAI). 2005:765–772.
21. Styner, M.; Oguz, I.; Xu, S.; Brechbuhler, C.; Pantazis, D.; Levitt, J.; Shenton, M.; Gerig, G. Framework for the statistical shape analysis of brain structures using spharm-pdm. Insight Journal, Special Edition on the Open Science Workshop at MICCAI; 2006.
22. Thompson PM, Hayashi KM, de Zubicaray G, Janke AL, Rose SE, Semple J, Hong MS, Herman DH, Gravano D, Doddrell DM, Toga AW. Mapping hippocampal and ventricular change in alzheimer disease. NeuroImage. 2004; 22:1754–1766. [PubMed: 15275931]
23. Van Reekum CM, Schaefer SM, Lapate RC, Norris CJ, Greischar LL, Davidson RJ. Aging is associated with positive responding to neutral information but reduced recovery from negative information. Social Cognitive and Affective Neuroscience. 2011; 6:177–185. [PubMed: 20385664]
24. Xu Y, Valentino DJ, Scher AI, Dinov I, White LR, Thompson PM, Launer LJ, Toga AW. Age effects on hippocampal structural changes in old men: the haas. NeuroImage. 2008; 40:1003–1015. [PubMed: 18280181]
25. Yu P, Grant PE, Qi Y, Han X, Segonne F, Pienaar R, Busa E, Pacheco J, Makris N, Buckner RL, et al. Cortical Surface Shape Analysis Based on Spherical Wavelets. IEEE Transactions on Medical Imaging. 2007; 26:582. [PubMed: 17427744]

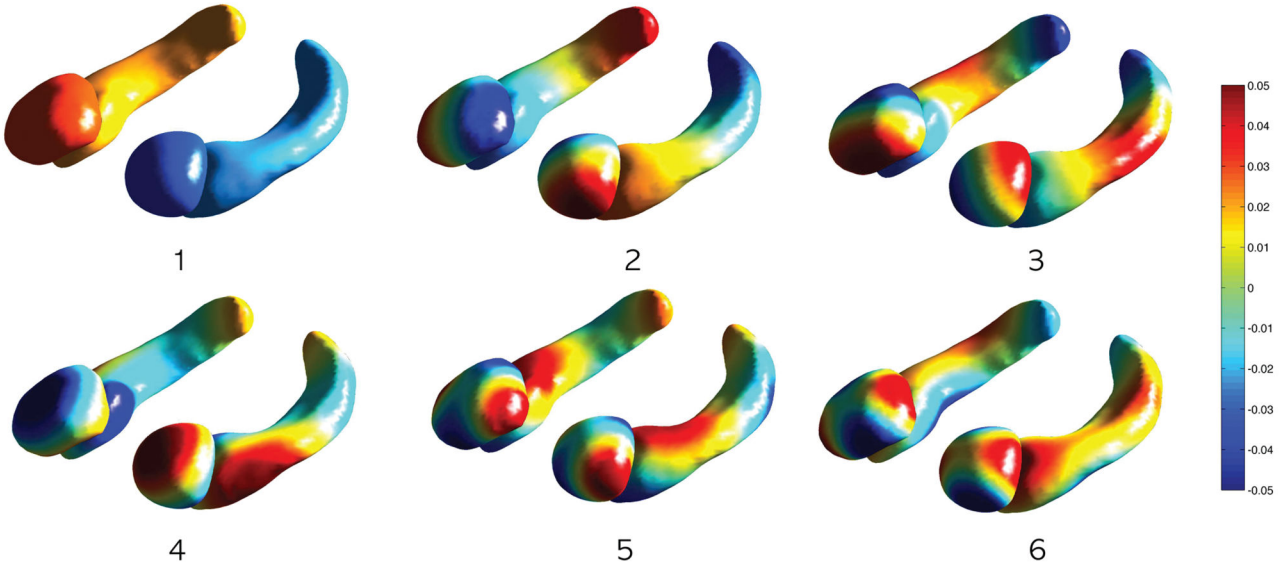

Figure 1.
First six Laplace-Beltrami eigenfunctions on amygdala and hippocampus surfaces.

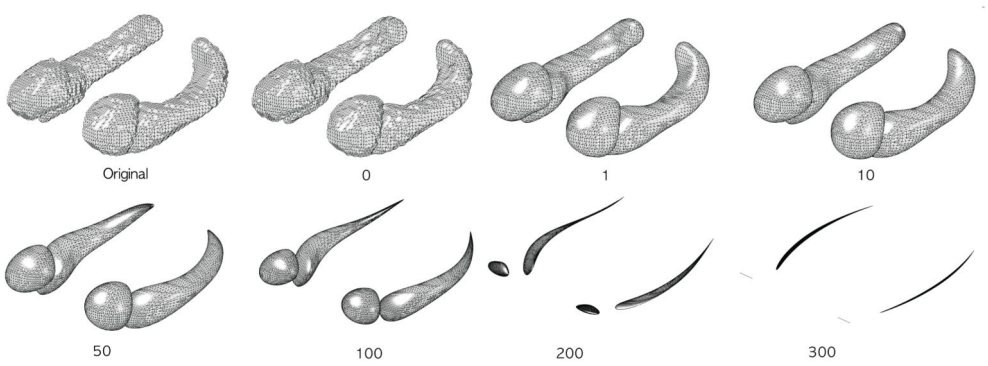

Figure 2.

Sparse shape representations for different sparse parameter λ. As λ increases, the shape itself becomes sparse. For sufficiently large λ, it represents the skeleton of the underlying shape. $\lambda = 1$ is used in the study.

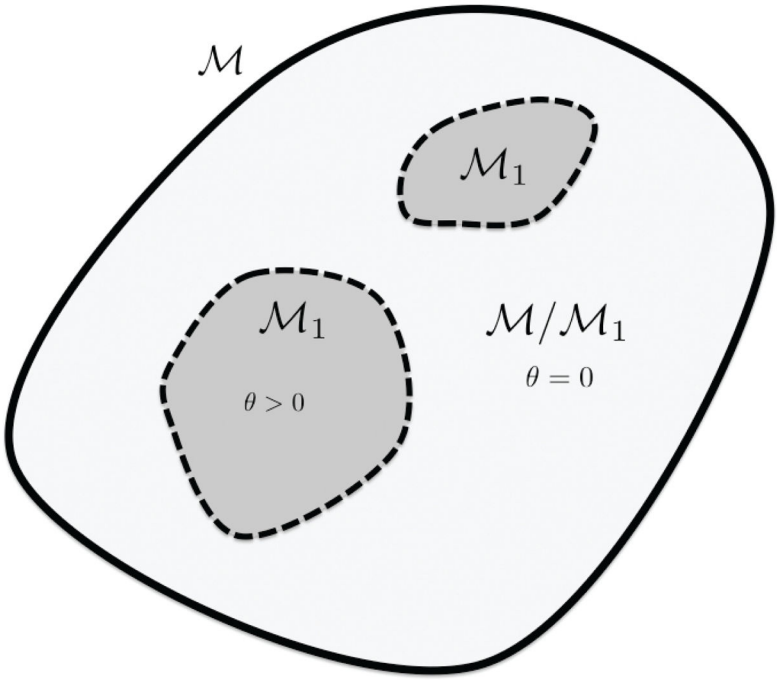

Figure 3.
Under H_1, there exist nonempty rejection regions $\mathcal{M}_1$ where the signal is significant, i.e. $\theta > 0$. The power is computed with respect to these rejection regions.

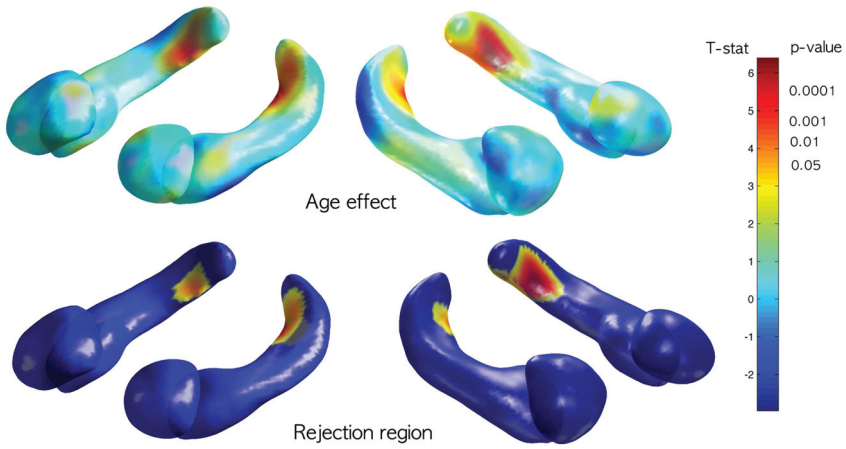

Figure 4.

Age effect on hippocampi. The T-statistic and the corrected *p*-value are shown. There is no age effect on the amygdalae. Rejection regions $\mathcal{M}_1$ corresponding to 0.05 level are also shown.

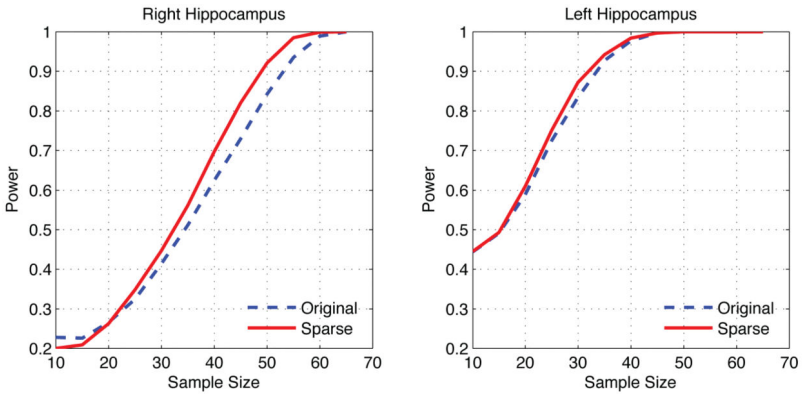

Figure 5.

Statistical power over sample size computed under multiple comparisons. The sparse regression increases statistical power.